

Carbene-Catalyzed Enantioselective Sulfonylation of Enone Aryl Aldehydes: A New Mode of Breslow Intermediate Oxidation

Rui Deng,^{a§} Shuquan Wu,^{a§} Chengli Mou,^{b§} Jianjian Liu,^a Pengcheng Zheng,^{a*} Xinglong Zhang^{d*} and Yonggui Robin Chi^{ac*}.

^aState Key Laboratory Breeding Base of Green Pesticide and Agricultural Bioengineering, Key Laboratory of Green Pesticide and Agricultural Bioengineering, Ministry of Education, Guizhou University, Huaxi District, Guiyang 550025, China.

^bSchool of Pharmacy, Guizhou University of Traditional Chinese Medicine, Huaxi District, Guiyang 550025, China.

^cDivision of Chemistry & Biological Chemistry, School of Physical & Mathematical Sciences, Nanyang Technological University, Singapore 637371, Singapore.

^dInstitute of High-Performance Computing, A*STAR (Agency for Science, Technology and Research), Singapore 138632, Singapore.

Content

I. General information	2
II. Preparation of substrates	3
III. Experimental section: condition optimization for the synthesis of 3a	4
IV. General procedure for the catalytic reactions	6
V. Mechanistic Studies	8
VI. LC-HRMS semi-quantitative analysis and ¹ H NMR of adduct 8	9
VII. The effect of added pTsOH instead of water	14
VIII. HRMS analysis of intermediates	15
IX. The rate of the NHC-catalyzed TsCl hydrolysis by LC-MS	16
X. Computational Methods	18
XI. Stereochemistry determination <i>via</i> X-ray crystallographic analysis	41
XII. References	42
XIII. Characterization of substrates and products	45
XIV. ¹ H NMR, ¹³ C NMR, ¹⁹ F NMR and HPLC spectra	69

X. Computational Methods

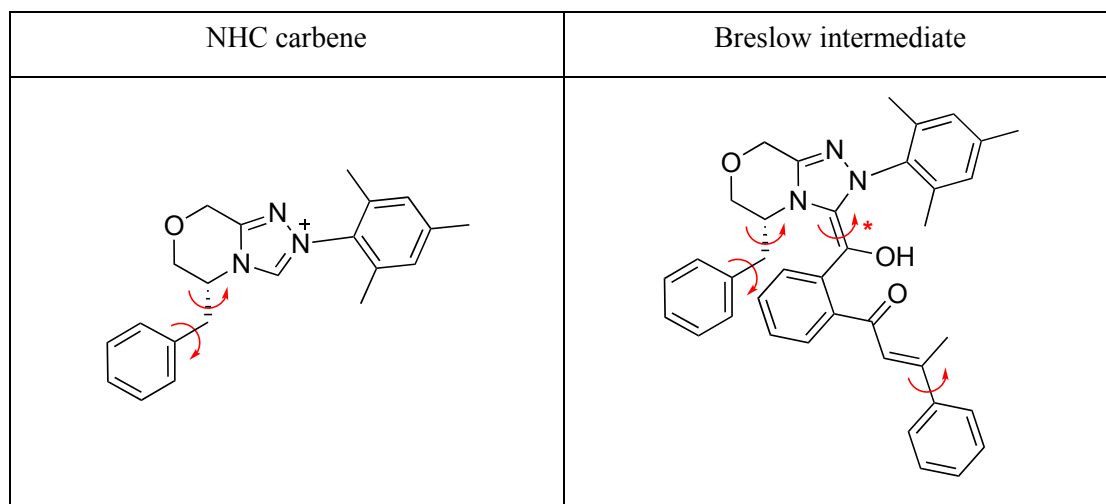
Geometry optimizations for conformational sampling in the gas phase were initially carried out using GFN2-xTB⁷ extended semiempirical tight-binding method in the *xtb* program^{8,9} from Grimme's group. The resulting cluster structures were further optimized using global hybrid functional M06-2X¹⁰ with Karlsruhe-family double- ζ valence def2-SVP^{11,12} basis set for all atoms as implemented in *Gaussian 16* rev. B.01.¹³ Single point (SP) corrections were performed using M06-2X functional and def2-TZVP¹¹ basis set for all atoms. Minima and transition structures on the potential energy surface (PES) were confirmed as such by harmonic frequency analysis, showing respectively zero and one imaginary frequency. The implicit SMD continuum solvation model¹⁴ for toluene solvent was used to account for the effect of solvent on the potential energy surface. Gibbs energies were evaluated at 30°C, which was used in the experiments, using a quasi-RRHO treatment of vibrational entropies.¹⁵ Vibrational entropies of frequencies below 100 cm⁻¹ were obtained according to a free rotor description, using a smooth damping function to interpolate between the two limiting descriptions.¹⁶ The free energies were further corrected using standard concentration of 1 mol/L for gas-phase-to-solvent correction.

For species involving open-shell characteristics, including radical ions in the redox potential calculations and closed-shell diradicaloid species in diradical coupling, we performed above-mentioned DFT methodologies using the unrestricted formalism of Kohn-Sham theory (UKS). Wavefunction stability in these cases were checked using Gaussian keyword "*stable=opt, guess=mix*". The eigenvalues of the spin operator S^2 after annihilation of spin contamination were checked to ensure that they comply with the expected value of $S(S+1) = 0.75$ for a doublet wavefunction and $S(S+1) = 0$ for closed shell diradical, indicating that spin contamination is not a problem for the present methodology.

Non-covalent interactions (NCIs) were analyzed using NCIPLOT¹⁷ calculations. The *.wfn* files for NCIPLOT were generated at M06-2X/def2-SVP level of theory. NCI indices calculated with NCIPLOT were visualized at a gradient isosurface value of $s = 0.5$ au. These are colored according to the sign of the second eigenvalue (λ_2) of the Laplacian of the density ($\nabla^2\rho$) over the range of -0.1 (blue = attractive) to +0.1 (red = repulsive). Molecular orbitals are visualized using an isosurface value of 0.05 au throughout. All molecular structures and molecular orbitals were visualized using *PyMOL* software.¹⁸

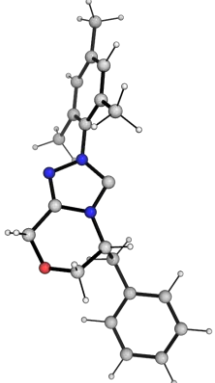
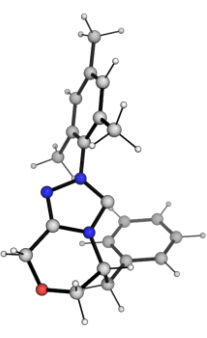
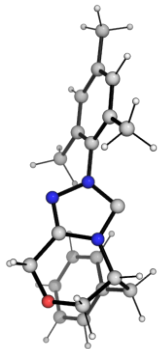
1. Conformational considerations

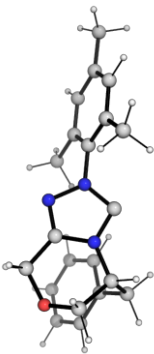
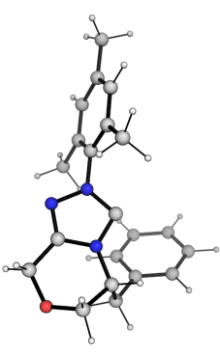
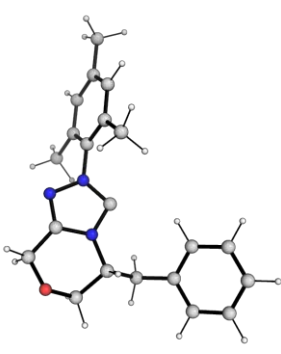
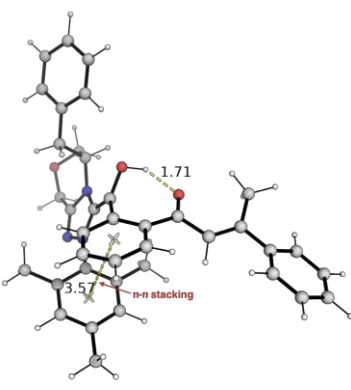
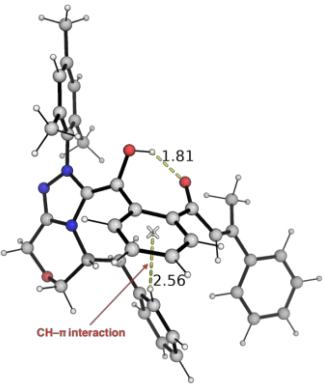
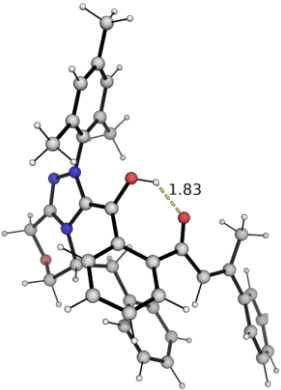
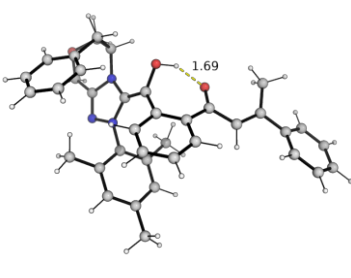
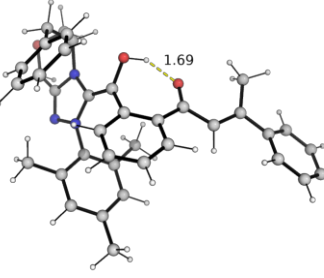
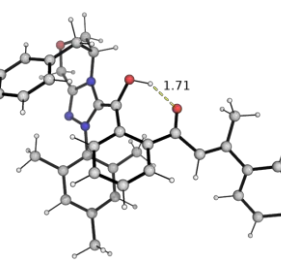
We determined the most stable form of the NHC carbene and the covalently formed Breslow intermediate (enol azolium) by performing a thorough conformational sampling. We generated a set of rotamers by performing 5-fold rotations about the key dihedral angles (in red) as shown in the Chemdraw structure in Scheme S-1.



Scheme S-1. Chemdraw structures of NHC carbene and azolium-enolate intermediate for which conformational samplings were performed by rotamer generation along bonds indicated by red arrows. For the latter structure, the rotation along the C=C bond (indicated by asterisk) is to account for all possible conformers that can arise from the initial NHC attack on either face of the aldehyde.

A total of 25 rotamers for NHC and 625 rotamers for the Breslow intermediate were generated and then cleaned by removing those species having overlapping atoms within 0.5 Å radius. These were performed using the script in the study of conformational effects on physical-organic descriptors by Brethomé *et al.*¹⁹ The resulting rotamers were subject to geometry optimization using GFN2-xTB method. The xTB-optimized structures were then clustered using the clustering_traj.py²⁰ with an RMSD cutoff of 1.0 Å (excluding H atoms) to give distinct conformers that were further optimized at DFT M06-2X/def2-SVP level. The Gibbs energies of the resulting structures were corrected using single-point M06-2x/def2-TZVP in toluene solvent using SMD implicit solvation model. Their DFT-optimized structures and relative solvent-corrected Gibbs energies are given in Figure S-12.

NHC carbene conformers		
NHC-c1	NHC-c2	NHC-c3
$\Delta G = 0.0$	2.6	2.6
		

NHC-c4	NHC-c5	NHC-c6
$\Delta G = 3.3$	3.6	4.5
		
Breslow intermediate I conformers		
I-c1	I-c2	I-c3
$\Delta G = 3.1$	4.6	5.0
		
I-c4	I-c5	I-c6
$\Delta G = 6.4$	6.7	8.0
		
I-c7	I-c8	I-c9
$\Delta G = 8.8$	9.0	9.1

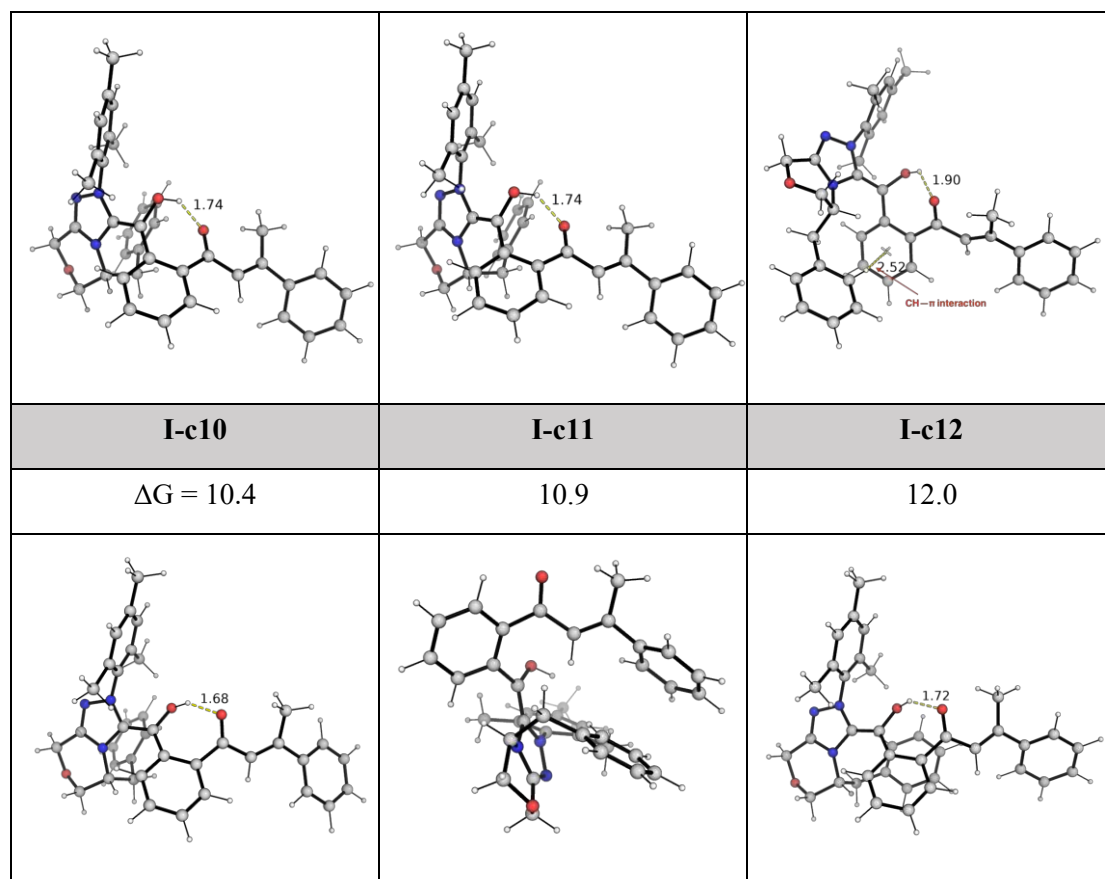


Figure S-12. DFT optimized conformer structures of NHC catalyst and Breslow intermediate **I**. Relative Gibbs energies are calculated at SMD (toluene)-M06-2X/def2-TZVP//M06-2X/def2-SVP level of theory and taken relative to the lowest energy conformer of the NHC carbene. For Breslow intermediate, the energies are taken relative to the sum of the lowest energy conformer of the NHC carbene and the enone aryl aldehyde substrate **1a**. Their units are given in kcal mol⁻¹.

2. Stereo-determining transition state (TS) structures

We compare the factors influencing the energetic differences between the stereo-determining TSs, *Re*-**TS5** and *Si*-**TS5**. Figure S-13 shows their DFT-optimized structures, frontier molecular orbitals (FMOs) and non-covalent interaction (NCI) plots. The HOMO and LUMO structures for both TSs are similar, indicating similar electronic influences. *Re*-**TS5** has a lower activation barrier due to the favorable NCIs between the C-H bonds on the aryl ring of the NHC and the O-atoms of Ts⁻ anion, which stabilize the transition state. These CH--O NCIs are absent in *Si*-**TS5**.

	<i>Re</i> - TS5	<i>Si</i> - TS5
ΔG^\ddagger	12.6 kcal mol ⁻¹	14.3 kcal mol ⁻¹

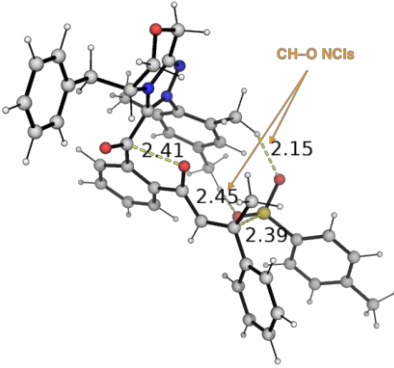
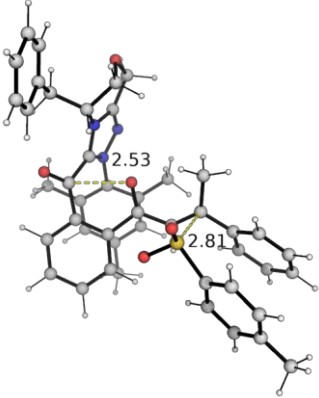
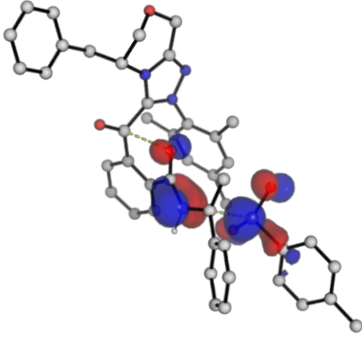
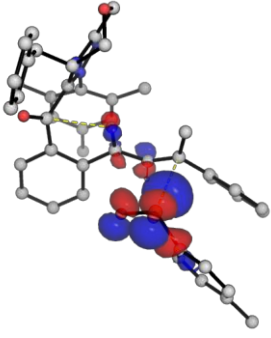
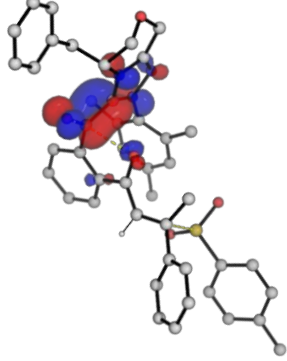
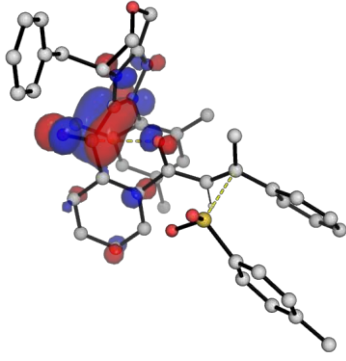
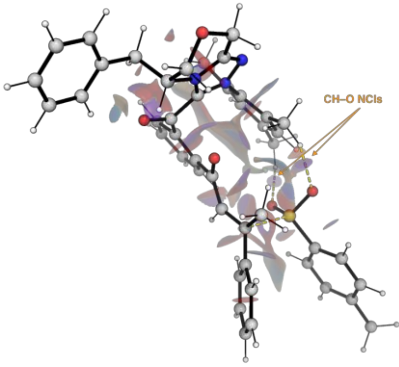
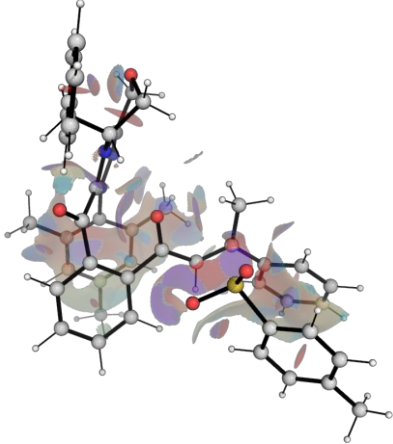

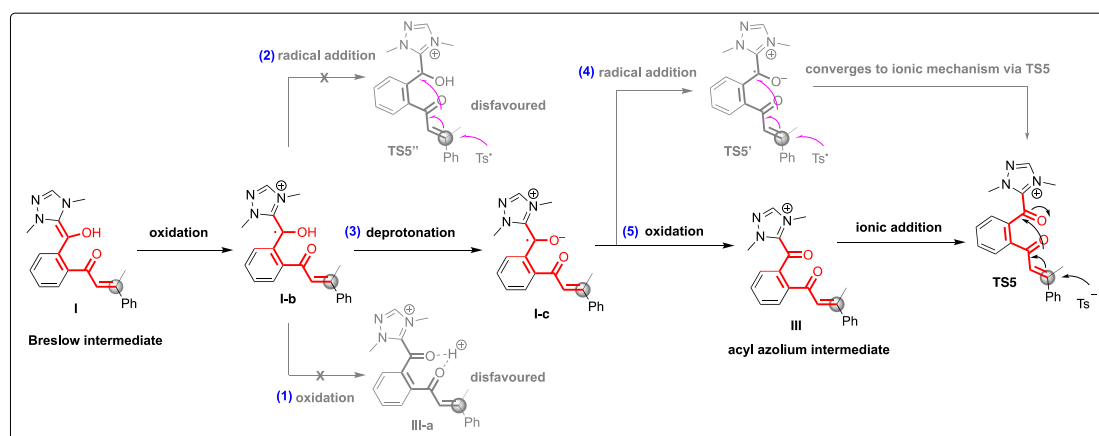
Optimized structure		
HOMO		
LUMO		
NCI		
NCI scale		

Figure S-13. Optimized TS structures, their FMOs (isosurface value = 0.05 au) and NCI plots for the stereo-determining transition states (**TS5s**) for the addition of Ts^- anion to acyl azolium intermediate **III** *via* ionic mechanism. Key bond distances are given in Å. Activation barriers are given in kcal mol⁻¹.

3. Redox chemistry/Radical mechanism

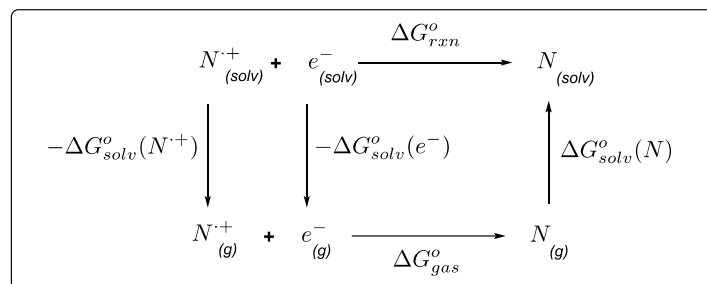
The alternative mechanism of the reaction *via* one-electron redox processes were investigated computationally. We considered the reaction pathways outlined in Scheme S-2. The Breslow intermediate **I** could undergo a single-electron oxidation to give **I-b**, which could undergo 3 possibilities: 1) further, second single-electron oxidation to give **III-a**; 2) direct radical addition with tosyl radical Ts^\bullet ; 3) deprotonation to give **I-c** followed by either (4) radical addition with Ts^\bullet or (5) further oxidation and subsequent addition by Ts^- *via* ionic mechanism. We carried out computational redox potential calculations to determine the feasibility of the catalytic transformation *via* redox chemistry.



Scheme S-2. Possible redox chemistry reaction pathways for Breslow intermediate **I**.

3.1 Computational redox potential calculations

To compute the electrochemical redox potentials of the species involved in the reaction, we applied the thermodynamic cycle as shown in Scheme S-3.^{21,22} We aim to calculate the Gibbs energy of reaction in the solvent phase, ΔG_{rxn}^o , using the structures we have optimized in the gas phase at M06-2X/def2-SVP level of theory. M06-2X functional has been shown to give good agreement between experimental and computed redox potentials.^{23,24}



Scheme S-3. Computational redox potential for the reduction of a radical cation to its neutral form *via* thermodynamic cycle.

In our calculations, the gas phase energy change, ΔG_{gas}^o , is further refined by calculating the single point energy in gas phase at a M06-2X/def2-TZVP for improved accuracy.²¹ The reduction potentials calculated here are *adiabatic* reduction potentials (ARP) since the energy is taken from each optimised species, i.e.,

$$\text{ARP} = E(\text{optimised neutral}) - E(\text{optimised radical cation}). \quad (1)$$

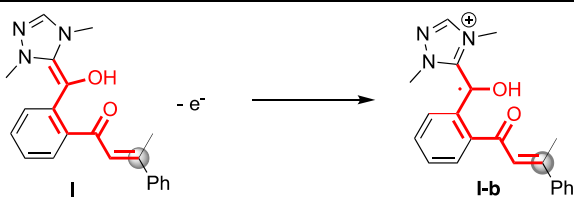
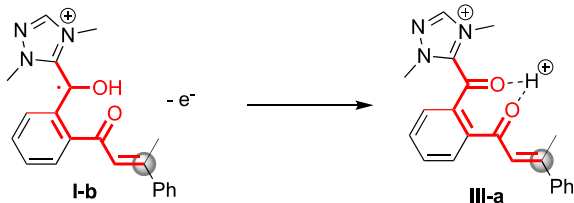
We then have

$$\Delta G_{rxn}^o = -\Delta G_{solv}^o(N^{\bullet+}) - \Delta G_{solv}^o(e^-) + \Delta G_{gas}^o(N^{\bullet+}) + \Delta G_{solv}^o(N) \quad (2)$$

The reduction potential of the reaction is then given by

$$E_{cell} = -\frac{\Delta G_{rxn}^o}{nF} - E_{SHE} \quad (3)$$

where the standard hydrogen electrode (SHE) redox value is taken as 4.28V in SMD model.^{21,22,25} We need not consider the free energy of solvation of the electron as their contribution cancels out when we consider the full reaction against experimentally measured values.²² The computed redox potentials for the chemical reactions are given in Table S-6.

Reaction	Oxidation	E_{ox}^o / V
O1		-0.193
O2		-1.958

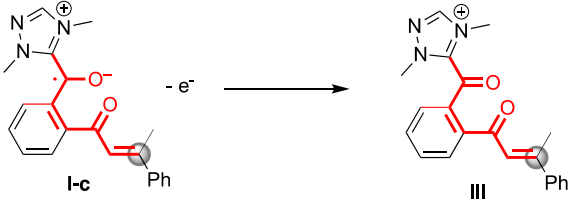
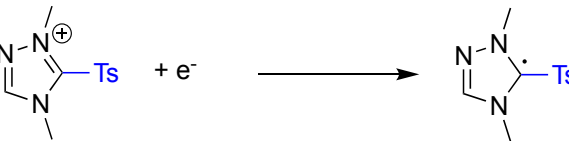
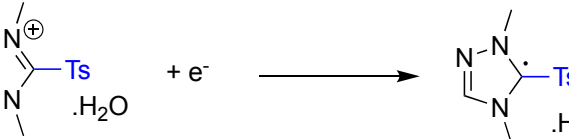
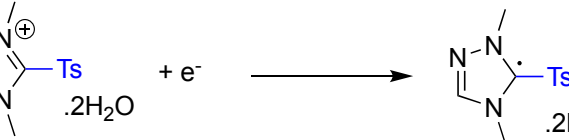
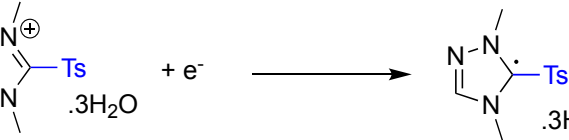

O3		+0.171
Reaction	Reduction	E_{red}° / V
R1	$TsOH + e^{-} \longrightarrow [TsOH]^{*-}$	-3.039
R2	$TsOH.H_2O + e^{-} \longrightarrow [TsOH.H_2O]^{*-}$	-3.139
R3	$TsOH.3H_2O + e^{-} \longrightarrow [TsOH.3H_2O]^{*-}$	-2.793
R4	$TsCl + e^{-} \longrightarrow [TsCl]^{*-}$	-1.533
R5	$Ts^{\bullet} + e^{-} \longrightarrow Ts^{-}$	-0.583
R6		-0.418
R7		-0.392
R8		-0.285
R9		-0.642
R10		-1.206

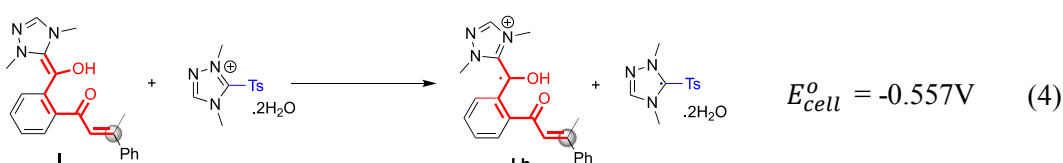
Table S-6. Computed redox potentials for the possible chemical transformations.

First redox event

From the table, the most likely oxidizing agent to oxidize Breslow intermediate **I** to intermediate **I-b** (reaction **O1**, $E_{ox}^{\circ} = -0.139$ V) is the $[\text{NHC-Ts}]^+$ complex that was detected experimentally. The reduction of $[\text{NHC-Ts}]^+$ complex to $[\text{NHC-Ts}]^{\bullet}$ can be enhanced in the presence of water, the reduction potential becomes less negative from -0.418V without water (reaction **R6**) to -0.285V with two water molecules (reaction **R8**).

The use of other species as oxidizing agents, such as TsOH (reactions **R1**, **R2** and **R3**) or TsCl (reaction **R4**) have more negative and unfavorable redox potentials than the reduction of $[\text{NHC-Ts.2H}_2\text{O}]^+$ complex.

The overall potential first redox transformation is thus:

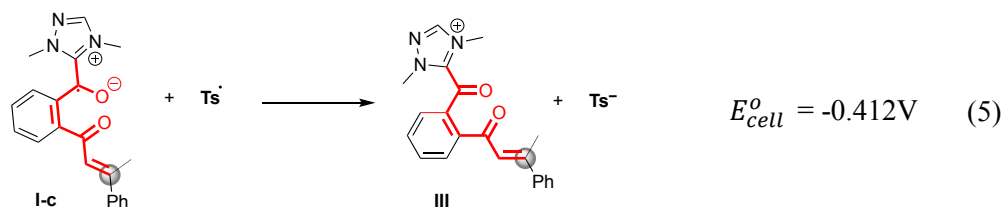


with an overall E_{cell}° of -0.557 V, this implies an uphill electron transfer barrier of about 12.8 kcal mol⁻¹.

Second redox event

The reduced $[\text{NHC-Ts.2H}_2\text{O}]^{\bullet}$ complex can dissociate to give Ts^{\bullet} radical, which can be reduced to Ts^- anion with $E_{red}^{\circ} = -0.583\text{V}$ (reaction **R5**, Table S-6).

The direct oxidation (loss of an electron) of radical cationic intermediate **I-b** to **III-a** has a large unfavorable redox potential of $E_{ox}^{\circ} = -1.958\text{V}$ (reaction **O2**, Table S-6). Thus, this rules out the pathway (1) in Scheme S-2. In the basic reaction condition, intermediate **I-b** can easily lose a proton to give intermediate **I-c** (pathway (2) in Scheme S-2), which can be oxidized to close-shell intermediate **III** much more easily, with $E_{ox}^{\circ} = +0.171\text{V}$ (reaction **O3**, Table S-6). This gives overall second redox transformation as



with an overall E_{cell}° of -0.412 V. This implies an uphill electron transfer barrier of about 9.5 kcal mol⁻¹.

3.2 Energy profile for redox chemistry

From the computational redox potential calculations, the reaction proceeding *via* redox events will have the Gibbs energy profile as shown in Figure S-14. The first redox event between $[\text{NHC-Ts}]^+.2\text{H}_2\text{O}$

complex and Breslow intermediate **I** will have an activation barrier of at least 11.0 kcal mol⁻¹ (with a small barrier for electron transfer²⁴). However, in the presence of both carbonate and TsCl, intermediate **I** will undergo a carbonate-assisted deprotonation of the OH group, forming an alkoxy group that gets tosylated with TsCl (as described in the main text). As such, we anticipate that the Breslow intermediate **I** will undergo tosylation readily with TsCl before it can get oxidized to intermediate **I-b** (Figure 2 in the main text).

For completeness, we investigated the mechanism for the radical coupling between the radical cationic intermediate **I-b** and Ts[•] radical (pathway (2) in Scheme S-2). From the reactant complex between **I-b** and Ts[•] radical (**INT1**^{••}), the barrier for the radical addition to the (*Re*)-face of intermediate **I-b** (**Re-TS5**^{••}) is 8.7 kcal mol⁻¹ and the barrier for the radical addition to the (*Si*)-face of intermediate **I-b** (**Si-TS5**^{••}) is 10.3 kcal mol⁻¹. Due to the reversibility of the formation of intermediate **I-b** and Ts[•] radical, the energetic span for this reaction pathway is at least 18.1 kcal mol⁻¹ (from the Breslow intermediate **I**). This is much less favorable than the main reaction pathway discussed in the main text.

Alternatively, species **I-b** can lose a proton to give species **I-c** (pathway (3), Scheme S-2), which can undergo redox event with Ts[•] radical (pathway (5), Scheme S-2) to give thermodynamically uphill acyl azolium intermediate **III** and Ts⁻ anion. The acyl azolium intermediate formed then undergoes ionic mechanism as discussed in the main text (Figure 2 in the main text).

The alternative mechanism from species **I-c** is its direct reaction with Ts[•] radical (pathway (4), Scheme S-2). However, the TS search using unrestricted closed-shell diradical formalism (on the singlet PES) converged to the ionic pathway in which Ts⁻ anion adds to the acyl azolium intermediate **III** (main mechanism in the main text). The unrestricted open-shell diradical TS search (on the triplet PES) between species **I-c** and Ts[•] radical yielded ³**Si-TS5**^{••} with a barrier of 17.4 kcal mol⁻¹ and ³**Re-TS5**^{••} with a barrier of 20.0 kcal mol⁻¹ (Figure S-14) and these are less kinetically favorable.

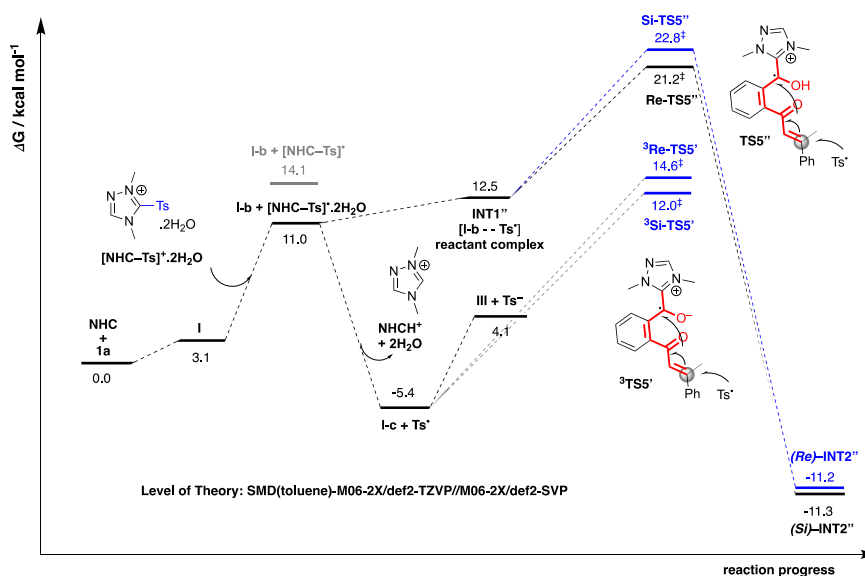


Figure S-14. Gibbs free energy profile calculated at SMD(toluene)-M06-2X/def2-TZVP//M06-2X/def2-SVP level of theory for redox chemistry.

4. Ionic mechanism

4.1 Addition of NHC to enone aryl aldehyde substrate

The transition state for the addition of NHC to either the (*Re*)- or the (*Si*)-face of aldehyde moiety of the substrate was found computationally. The DFT optimized structures are given in Figure S-15.

	<i>Re</i> -TS1	<i>Si</i> -TS1
ΔG^\ddagger	20.6 kcal mol ⁻¹	25.0 kcal mol ⁻¹
Optimized structure		

Figure S-15. DFT optimized structures for the addition of NHC to aldehyde substrate.

4.2 Formation of Breslow intermediate I

Due to the highly (*Re*)-face selective addition of NHC, for subsequent transformations, we follow the mechanistic pathways from the reaction product resulting from (*Re*)-face addition. In accordance with previous reports,^{26,27} a protonated base assists in the formation of the Breslow intermediate. Herein, we used hydrogen carbonate in the transition state search and the DFT optimized structures and their associated energy barriers are shown in Figure S-16.

S-TS2	S-TS2-c2	S-TS2-c3
$\Delta G^\ddagger = 22.4$ kcal mol ⁻¹	37.0 kcal mol ⁻¹	42.1 kcal mol ⁻¹

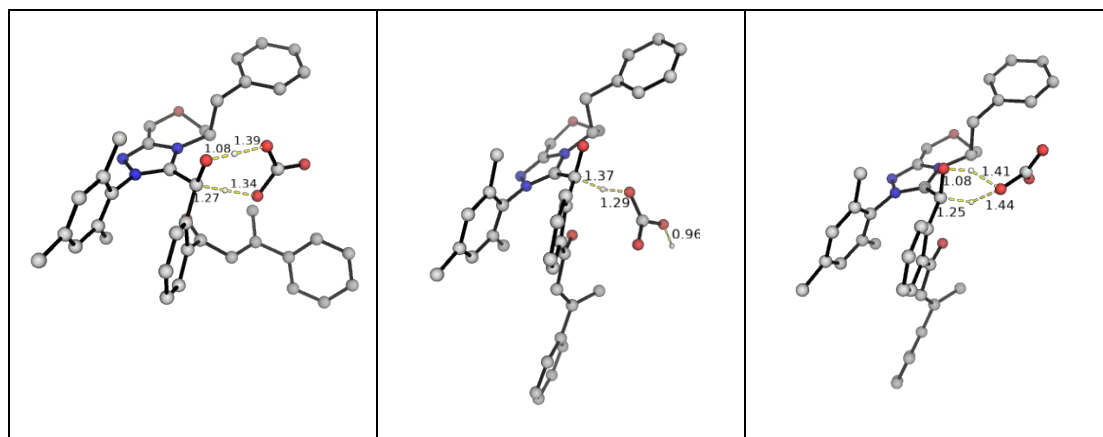


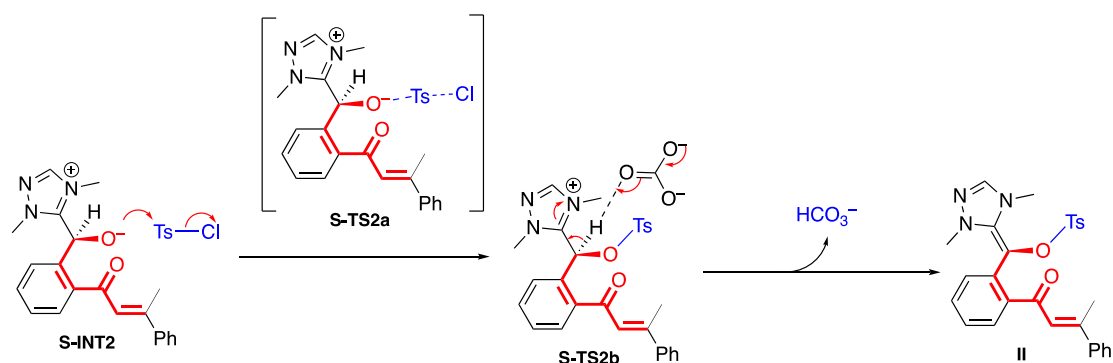
Figure S-16. DFT optimized structures for the hydrogen carbonate assisted formation of Breslow intermediate from NHC addition product.

We see that the concerted deprotonation and reprotonation by hydrogen carbonate *via* a highly ordered 7-membered ring transition state **S-TS2** has the lowest activation barrier of 22.4 kcal mol⁻¹, whereas the direct deprotonation *via* **S-TS2-c2** and the deprotonation by the same carboxyl oxygen *via* **S-TS2-c3** with a 5-membered ring TS both have much higher barriers at 37.0 and 42.1 kcal mol⁻¹ respectively.

4.3 Alternative mechanism for the direct tosylation of NHC-adduct oxyanion without the formation of Breslow intermediate I

We computationally investigated the mechanistic alternative for the direct formation of intermediate **II** by direct tosylation of NHC-adduct, without the formation of Breslow intermediate **I** (Scheme S-4).

We successfully located and verified the transition state for the direct tosylation at the oxyanion oxygen atom (**S-TS2a**). The solvent-corrected Gibbs energy profile is shown in Figure S-17.



Scheme S-4. Alternative mechanism for the formation of intermediate **II** *via* direct tosylation of NHC adduct.

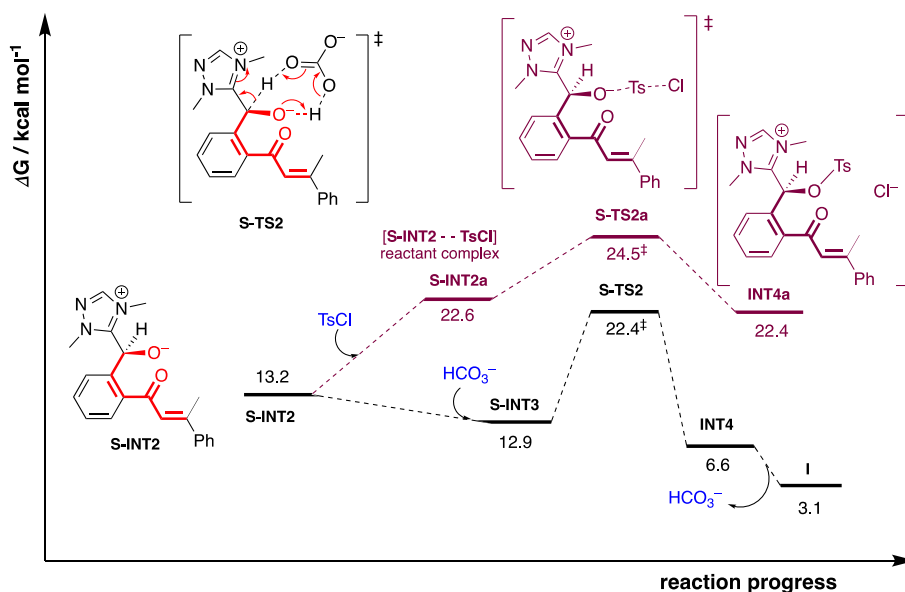


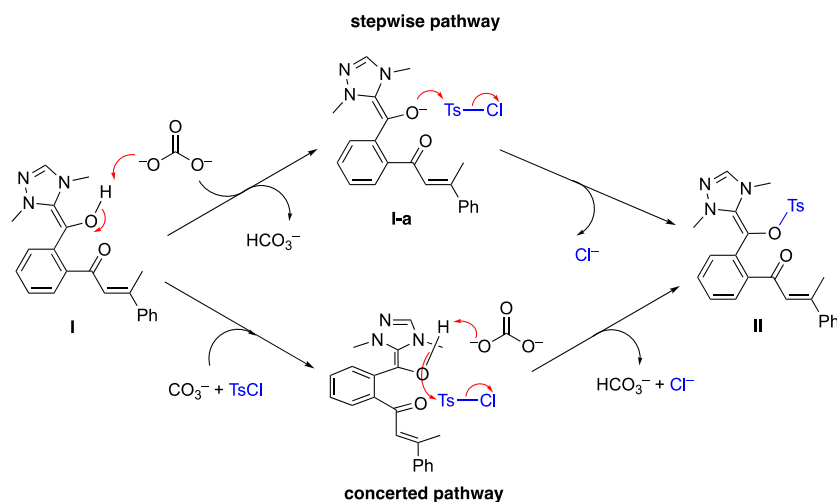
Figure S-17. Gibbs free energy profile for the direct tosylation of oxyanion from NHC adduct (**S-TS2a**) and its comparison to the transition state for the base-assisted Breslow intermediate formation (**S-TS2**).

We see that the direct tosylation of the oxyanion oxygen (**S-TS2a**) has a higher barrier than the base-assisted formation of Breslow intermediate **I** via **S-TS2**. This barrier difference $\Delta\Delta G^\ddagger$ of 2.1 kcal mol⁻¹ translates to about 33:1 kinetic favorability for **S-TS2** over **S-TS2a**, using simple transition state theory at the reaction temperature. Similar mechanism to what we proposed in our manuscript for base-assisted Breslow intermediate formation in carbene organocatalysis have been reported by Donghui Wei, Yu Lan and co-workers.^{26,27}

In addition and more importantly, intermediates **I** and **I-a** have been successfully detected experimentally, for the first time, using high-resolution mass spectroscopy (HRMS), under positive ion and negative ion mode, respectively. These intermediates would not have been formed via this mechanistic alternative of direct tosylation of NHC-adduct. This provides unequivocal evidence for the formation of the Breslow intermediate and is in direct support of the mechanism we proposed in the main text.

4.4 Conversion of Breslow intermediate **I** to intermediate **II**

We explore both the concerted pathway and the stepwise pathway for the conversion of intermediate **I** to intermediate **II** as shown in Scheme S-5.



Scheme S-5. Stepwise vs concerted mechanistic pathway for the conversion of intermediate **I** to intermediate **II**.

In the stepwise pathway, carbonate anion deprotonates the alcohol group of the Breslow intermediate **I**, giving the alkoxide **I-a**, which subsequently undergoes tosylation with tosyl chloride to give tosylated intermediate **II**. We found that the deprotonation of intermediate **I** by carbonate anion is barrierless, as can be seen from the geometry optimization shown in Figure S-18. From an initial guess where the carbonate is placed far away from the NHC adduct (O(carbonate)-H(hydroxyl) distance of 3.5Å, structure **1**, Figure S-18), the geometry optimization gave the deprotonated product (structure **81**, Figure S-18) directly, indicating that no barriers exist for the deprotonation of hydroxyl group of NHC adduct by carbonate anion.

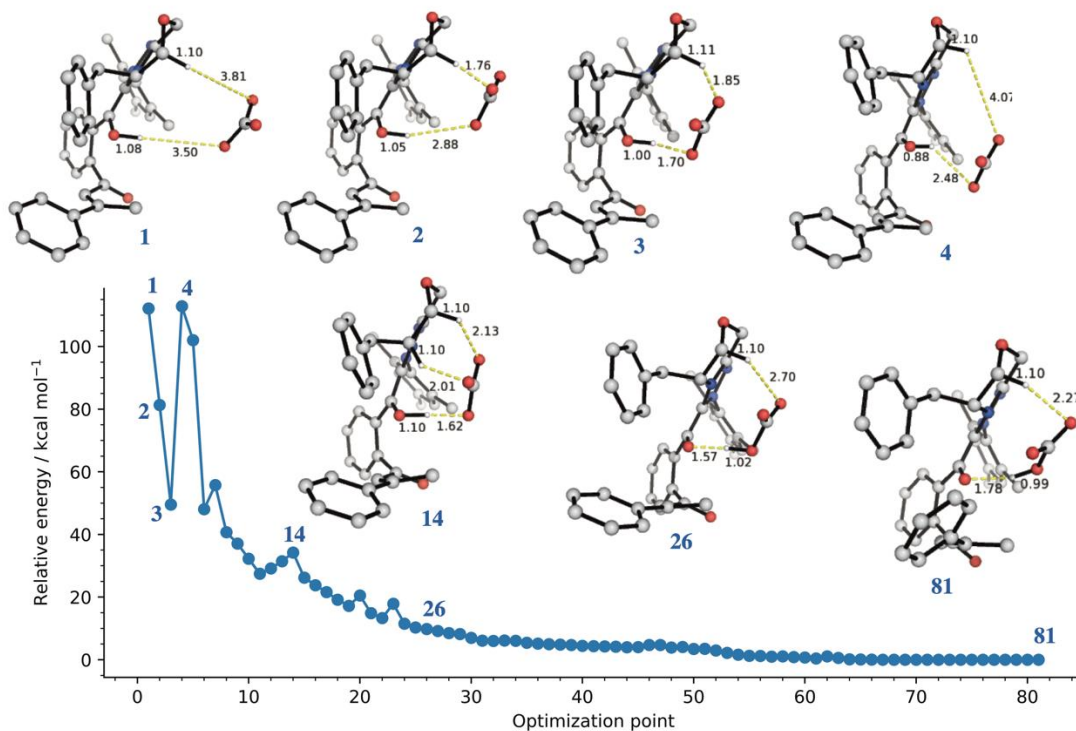
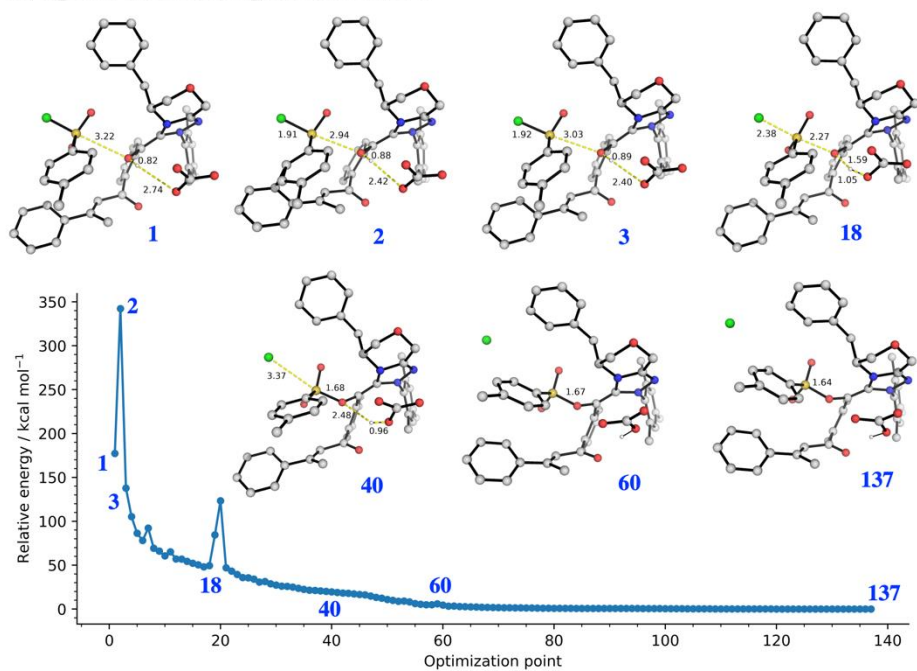


Figure S-18. Geometry optimization of carbonate anion and the Breslow intermediate **I** starting from guess structure **1**. Shown are selected structures along the optimization. Structure **81** is the DFT optimized structure. Selected bond distances are given in Å.

In the concerted pathway, carbonate anion deprotonates the alcohol group of the Breslow intermediate while the deprotonated alkoxide attacks the sulfur center of TsCl in an S_N2 mechanism as chloride leaves, much similar to a general base catalysis. The direct TS search did not yield any transition structure. The optimization of initial guess structure **1** in Figure S-19a) gives the tosylated intermediate **II** directly. However, with a larger O (Breslow intermediate)-S distance as in guess structure **1'** in Figure S-19b, the direct optimization did not yield the tosylated intermediate **II** directly, although spontaneous deprotonation of the alcohol group by carbonate is still observed. This suggests that the conversion of intermediate **I** to intermediate **II** is likely stepwise, with firstly a barrierless deprotonation of OH group of **I** followed by subsequent tosylation of the alkoxide with TsCl.

a) Optimization from guess structure 1



b) Optimization from guess structure 1'

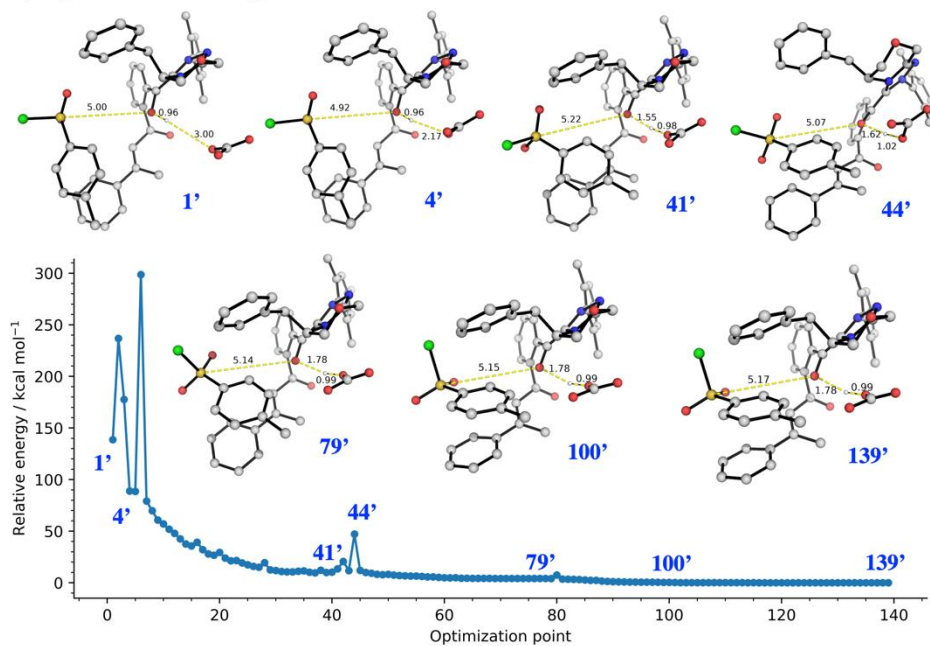
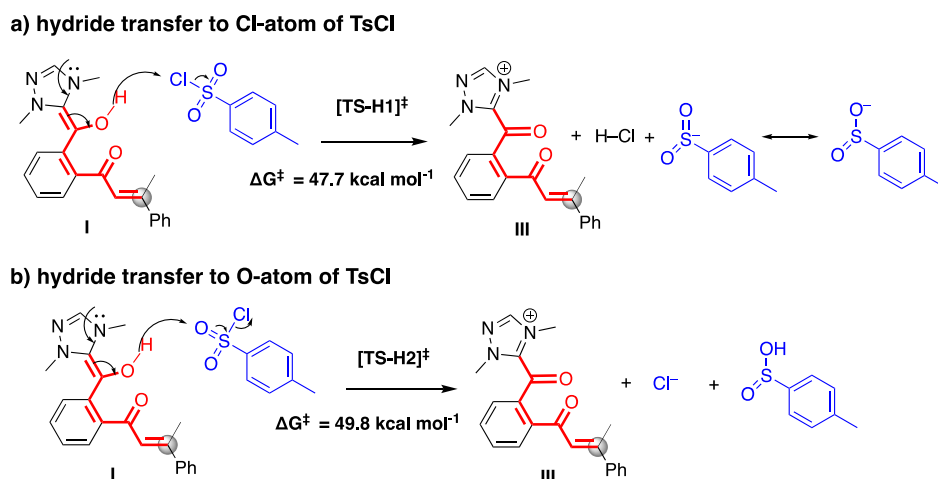


Figure S-19. Geometry optimizations of concerted carbonate anion-assisted deprotonation and tosylation of the Breslow intermediate **I** starting from guess structure **1** (a; top panel) and guess structure **1'** (b; bottom panel). Shown are selected structures along the optimization. Structures **137** and **139** are the DFT optimized structures. Selected bond distances are given in Å.

4.5 Alternative mechanism for the generation of Ts⁻ anion *via* hydride transfer

The alternative mechanism for the generation of tosyl anion Ts⁻ *via* hydride transfer from the Breslow intermediate **I** is also considered (Scheme S-6). These TSs (hydride transfer to either the Cl-atom or the O-atom of TsCl), shown in Figure S-20, have very high barriers (47.7 kcal mol⁻¹ and 49.8 kcal mol⁻¹, respectively) and are thus highly disfavored.



Scheme S-6. Possible reaction pathways for the generation of tosyl anion *via* hydride transfer.

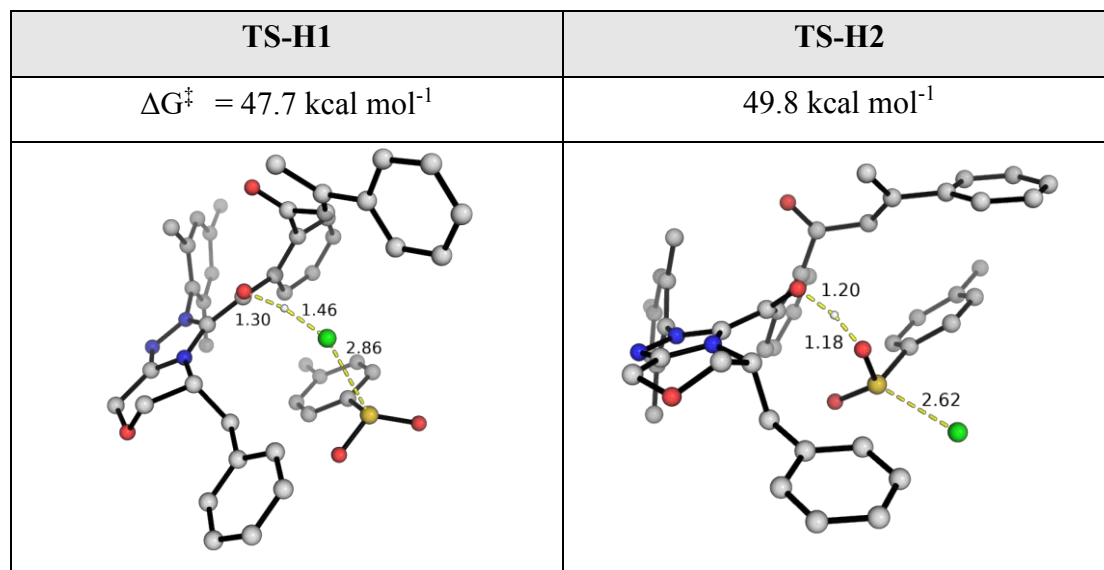
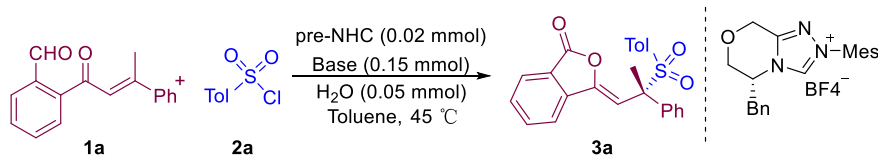


Figure S-20. DFT optimized structures for the generation of Ts⁻ anion *via* hydride transfer.

4.6. The roles of bases in key steps were further studies *via* experiments and DFT calculation

With an optimal reaction condition in hand, we tested the effect of bases other than carbonate due to the central role in the mechanism as **INT5**. We observe that the identity of the base does not drastically affect the ee values. This suggests that the base does not participate in the stereo-determining step and is consistent with our computed mechanism showing that the stereo-determining step only involves the addition of Ts⁻ anion to the acyl azolium intermediate, without any base participation.



Bases	Yield (%) ^a	Ee (%) ^b
DBU	21	98
Et ₃ N	15	98
DABCO	nr	nr
K ₃ PO ₄	34	94
KOAc	< 10	98
t-BuOK	22	90

Unless otherwise specified, the reactions were carried using **1a** (0.1 mmol), **2a** (0.12 mmol), pre-NHC (0.02 mmol), base (0.15 mmol), Toluene (2.0 mL) and H₂O (0.05 mmol) at 45 °C for 4 h. ^aIsolated yield of **3a**. ^bThe ee values were determined *via* HPLC on chiral stationary phase. DBU = 1,8-Diazabicyclo[5.4.0]undec-7-ene. Et₃N = Triethylamine. DABCO = 1,4-Diazabicyclo[2.2.2]octane; triethylenediamine. KOAc = Potassium Acetate. t-BuOK = Potassium tert-butoxide. nr = no reaction.

The roles of the base in our reaction are three folds: 1) to deprotonate the NHC pre-catalyst to form the NHC singlet carbene active catalyst; 2) to participate in the base- (or its conjugate acid-) assisted formation of Breslow intermediate from NHC-aldehyde adduct (**S-TS2** in our reaction); and 3) to participate in the deprotonation of Breslow intermediate to form its enolate equivalent which subsequently undergoes tosylation to give intermediate **II**.

Preliminary DFT studies were carried out to investigate how the base may affect the yield of the present transformation. For bases DBU, Et₃N and DABCO, thermodynamics calculations showed that the complex formation between the base and the Breslow intermediate **I** is uphill by more than 10 kcal mol⁻¹ (DBU 11.6 kcal mol⁻¹, Et₃N 11.4 kcal mol⁻¹ and DABCO 10.6 kcal mol⁻¹). In addition, the geometry optimization using deprotonated product (**I-a** and HNR₃⁺) as the initial guess structure (with O-H bond distance of 2 Å and H-N distance of 1 Å, Figure S-21a below) yields the Breslow intermediate **I** and the neutral amine base. This suggests that the deprotonation of Breslow intermediate by these nitrogenous amines is highly reversible, with equilibrium lying to the Breslow intermediate **I** (Figure S-21b below). Thus, no barrierless deprotonation at this step by these bases are possible, explaining the poor yields observed experimentally for these bases.

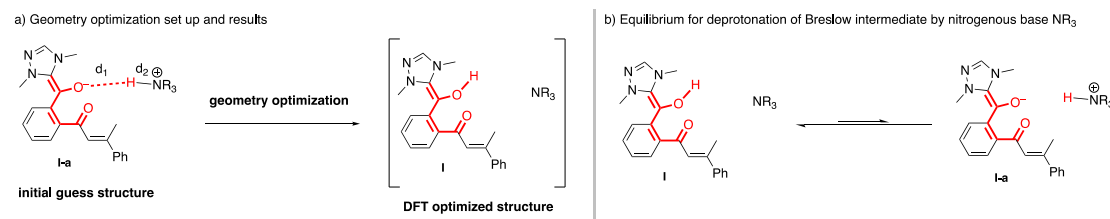


Figure S-21. DFT for the deprotonation of Breslow intermediate

For strong base tBuOK, although the barrierless deprotonation of Breslow intermediate **I** is observed computationally (as expected, as t-BuO⁻ is a much stronger base than CO₃²⁻), however, its conjugate acid t-BuOH is very weak. The participation of tBuOH in the Breslow intermediate formation (as compared

to HCO_3^-) is highly disfavored. The computed Gibbs energy for this process is shown in the Figure below:

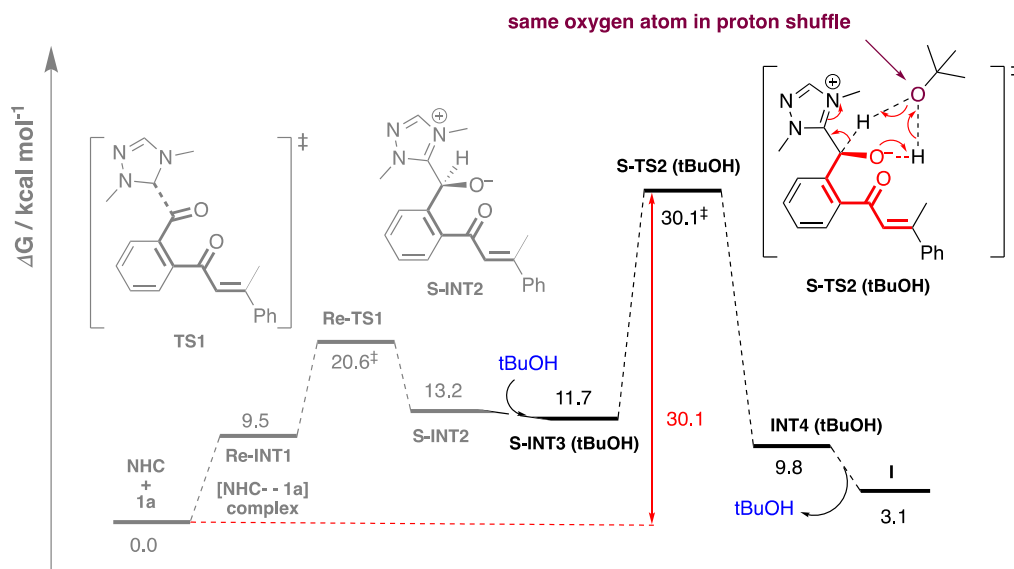


Figure S-22. Gibbs energy profile for tBuOK-assisted to generate Breslow intermediate.

This process is highly disfavored for two reasons: 1) this weak conjugate acid makes the breaking of O-H bond difficult, thus making it a poor proton shuffler, and 2) the involvement of the same oxygen atom in the cyclic transition state (**S-TS2(tBuOH)**) is less favored than if two *different* O atoms are involved, as in the case of hydrogen carbonate in **S-TS2**. This effect is similarly observed when only one oxygen atom of hydrogen carbonate was used (**S-TS2-c3**, Figure S-16), as demonstrated in Figure S-23.

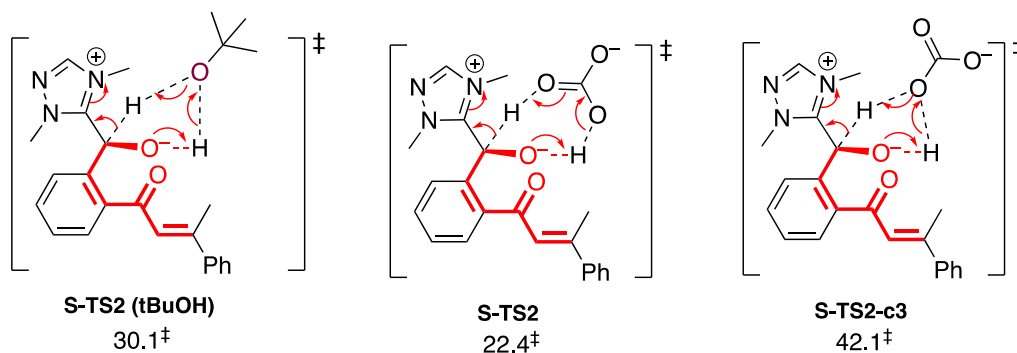


Figure S-23. The barrier of the proton transfer to form Breslow intermediate with different bases

For acetate and phosphate bases, preliminary DFT calculations suggested that the poor yields may not be due to their poor participation in the deprotonat base-assisted formation of Breslow intermediate (role 2) and in the deprotonation of Breslow intermediate to form its enolate equivalent (role 3). They may be less efficient than carbonate in generating the active NHC from the triazolium pre-catalyst (role 1). Additional detailed investigations on the roles of bases affecting various steps in this reaction are currently underway in our laboratory.

5. Optimized structures and absolute energies, zero-point energies

Geometries of all optimized structures (in .xyz format with their associated energy in Hartrees) are included in a separate folder named *final_xyz_structures*. All these data have been uploaded to zenodo.org (DOI: 10.5281/zenodo.5889602).

Absolute values (in Hartrees) for SCF energy, zero-point vibrational energy (ZPE), enthalpy and quasi-harmonic Gibbs free energy (at 303.15K) for M06-2X/def2-SVP optimized structures are given below. Single point corrections in SMD (toluene) using M06-2X/def2-TZVP functional are also included.

Structure	E/au	ZPE/au	H/au	T.S/au	qh-G/au	SP M06-2X/def2TZVP
1a	-805.731571	0.264746	-805.448951	0.061849	-805.50766	-806.6467343
TsCl	-1278.93909	0.130338	-1278.796842	0.048432	-1278.84314	-1279.780193
TsCl_ra	-1278.993608	0.127551	-1278.853314	0.05113	-1278.902266	-1279.87654
nhc_Ts	-1871.02858	0.537212	-1870.457171	0.099698	-1870.548503	-1872.912768
nhc_Ts_rad						
ical	-1871.203581	0.534835	-1870.634459	0.099121	-1870.726137	-1873.052055
nhc_Ts_ra	-1871.275795	0.532019	-1870.708819	0.101826	-1870.801709	-1873.161667
nhc_Ts_H2						
O	-1947.368323	0.561012	-1946.769325	0.108232	-1946.868262	-1949.347453
nhc_Ts_H2						
O_radical	-1947.544244	0.559813	-1946.946995	0.105758	-1947.044595	-1949.489907
nhc_Ts_2H						
2O	-2023.710935	0.586096	-2023.083687	0.115341	-2023.188743	-2025.78802
nhc_Ts_2H						
2O_radical	-2023.890783	0.58595	-2023.264598	0.113372	-2023.367889	-2025.935547
nhc_Ts_3H						
2O	-2100.083072	0.613317	-2099.426778	0.116807	-2099.534141	-2102.246185
nhc_Ts_3H						
2O_radical	-2100.248116	0.612463	-2099.593572	0.11557	-2099.699872	-2102.37919
Cl_anion	-460.067961	0	-460.065561	0.014629	-460.08019	-460.3216879
TsOH	-894.635635	0.14394	-894.479849	0.047287	-894.525367	-895.4191102
TsOH_ra	-894.634368	0.139603	-894.482428	0.048457	-894.529396	-895.4594056
Ts_radical	-818.86639	0.127222	-818.728557	0.044992	-818.7722	-819.5386707
Ts_anion	-818.947812	0.125716	-818.811366	0.044683	-818.854594	-819.6735503
TsO_anion	-894.105011	0.131823	-893.9619	0.047101	-894.006785	-894.9462024

TsOH_H2						
O	-970.989144	0.169728	-970.805205	0.052282	-970.855403	-971.8671387
TsOH_H2						
O_ra	-970.986143	0.165612	-970.80555	0.055096	-970.858114	-971.9033566
OH_anion	-75.63046	0.008034	-75.619066	0.016888	-75.635954	-75.84411311
H2O	-76.323214	0.021594	-76.297776	0.018768	-76.316544	-76.43033506
H2O_ra	-76.186163	0.015457	-76.166853	0.01964	-76.186493	-76.3927995
nhc_Ts_Cl	-2331.271845	0.536888	-2330.698776	0.102937	-2330.793628	-2333.282309
nhc_Ts	-1871.02858	0.537212	-1870.457171	0.099698	-1870.548503	-1872.912768
HCl	-460.637287	0.006845	-460.627083	0.018515	-460.645598	-460.8017807
carbonate	-263.302341	0.014746	-263.28342	0.027119	-263.310539	-263.8833848
hydrogen_c						
arbonate	-264.138182	0.027396	-264.106287	0.027639	-264.133927	-264.5283622
nhc	-1052.302221	0.405021	-1051.873311	0.07661	-1051.944345	-1053.495727
nhc_c2	-1052.299223	0.404748	-1051.870571	0.077106	-1051.941742	-1053.491192
nhc_c3	-1052.302507	0.405081	-1051.873684	0.07537	-1051.943925	-1053.492206
nhc_c4	-1052.302507	0.405079	-1051.874389	0.073459	-1051.942856	-1053.492205
nhc_c5	-1052.299224	0.404724	-1051.871534	0.073108	-1051.940158	-1053.491192
nhc_c6	-1052.296896	0.404965	-1051.867954	0.077201	-1051.939352	-1053.488265
I	-1858.083221	0.673815	-1857.368329	0.114792	-1857.472897	-1860.166086
I_c2	-1858.080924	0.673949	-1857.366012	0.112797	-1857.469602	-1860.16462371
I_c3	-1858.081426	0.673989	-1857.366573	0.113228	-1857.470434	-1860.163654
I_c4	-1858.083438	0.674298	-1857.368338	0.112824	-1857.471829	-1860.162042
I_c5	-1858.081099	0.673631	-1857.366426	0.11364	-1857.470502	-1860.160624
I_c6	-1858.082899	0.674345	-1857.369009	0.109949	-1857.469742	-1860.161073
I_c7	-1858.075809	0.674113	-1857.360794	0.11577	-1857.465597	-1860.156817
I_c8	-1858.075811	0.674099	-1857.360812	0.115171	-1857.465321	-1860.156786
I_c9	-1858.068459	0.673244	-1857.353826	0.116596	-1857.459391	-1860.155234
I_c10	-1858.071621	0.67365	-1857.356879	0.116173	-1857.462137	-1860.15352

I_c11	-1858.073802	0.673086	-1857.360632	0.109844	-1857.461688	-1860.155467
I_c12	-1858.070678	0.673078	-1857.356499	0.113576	-1857.460417	-1860.151747
I-a	-1857.520507	0.659356	-1856.82045	0.111287	-1856.923182	-1859.637919
I-b	-1857.88792	0.673842	-1857.173141	0.116088	-1857.278542	-1860.000776
I-c	-1857.480264	0.662457	-1856.777271	0.112875	-1856.880898	-1859.562497
II	-2676.395295	0.793284	-2675.550977	0.135208	-2675.674058	-2679.142703
III	-1857.301007	0.663773	-1856.596672	0.111864	-1856.699773	-1859.413372
Re-INT1	-1858.067215	0.672244	-1857.353241	0.11406	-1857.458385	-1860.154344
Re-TS1	-1858.055137	0.673349	-1857.34154	0.111225	-1857.443812	-1860.139225
Re-INT1	-1858.067215	0.672244	-1857.353241	0.11406	-1857.458385	-1860.154344
Re-TS1	-1858.055137	0.673349	-1857.34154	0.111225	-1857.443812	-1860.139225
S-INT2	-1858.068099	0.674912	-1857.353043	0.110413	-1857.454935	-1860.152731
S-INT3	-2122.267003	0.703169	-2121.518957	0.119588	-2121.629799	-2124.70143
S-TS2	-2122.251111	0.697627	-2121.50934	0.117779	-2121.618527	-2124.681709
S-TS2-c2	-2122.224055	0.697653	-2121.481617	0.120884	-2121.592534	-2124.65731
S-TS2-c3	-2122.201492	0.697344	-2121.459731	0.12073	-2121.570381	-2124.648806
INT4	-2122.284598	0.702351	-2121.536663	0.122756	-2121.649352	-2124.709483
INT5	-2121.625306	0.688215	-2120.891894	0.12038	-2121.003293	-2124.14523
INT6	-3136.482731	0.790578	-3135.638768	0.14171	-3135.766658	-3139.420557
TS-3	-3136.474582	0.790529	-3135.631467	0.13803	-3135.757333	-3139.406645
INT7	-3136.522091	0.793366	-3135.675632	0.139579	-3135.802889	-3139.473786
TS4	-2676.366913	0.790691	-2675.525077	0.135519	-2675.648465	-2679.103741
INT8	-2676.409815	0.791888	-2675.566926	0.133943	-2675.689746	-2679.138278
INT9	-2676.407169	0.792905	-2675.563096	0.135924	-2675.686924	-2679.14758
INT9''	-2676.780787	0.802193	-2675.926033	0.143592	-2676.053991	-2679.549241
Re-TS5	-2676.387713	0.792285	-2675.545029	0.133419	-2675.666927	-2679.128092
Re-TS5'	-2676.387714	0.792304	-2675.545023	0.133364	-2675.666885	-2679.128093
Re-TS5''	-2676.770573	0.802113	-2675.917207	0.138241	-2676.041615	-2679.537628

Re-TS5''-c2	-2676.766138	0.802153	-2675.912836	0.1389	-2676.037517	-2679.535744
S-INT10	-2676.411065	0.794989	-2675.566321	0.131575	-2675.686622	-2679.155511
S-INT10''	-2676.778404	0.804097	-2675.923099	0.137086	-2676.046915	-2679.547719
S-INT11	-2676.419531	0.79364	-2675.575151	0.135316	-2675.69788	-2679.165517
Si-TS5	-2676.370061	0.790975	-2675.527968	0.13826	-2675.652356	-2679.122369
Si-TS5'	-2676.377433	0.791921	-2675.53469	0.137874	-2675.6584	-2679.124027
Si-TS5''	-2676.766808	0.801962	-2675.914489	0.136927	-2676.037545	-2679.535269
Si-TS5''-c2	-2676.769773	0.802392	-2675.916305	0.137717	-2676.040343	-2679.535208
S-INT2a	-3137.033554	0.806411	-3136.174327	0.138863	-3136.300897	-3139.941611
S-TS2a	-3137.035574	0.80665	-3136.177082	0.135947	-3136.301489	-3139.939997
INT4a	-3137.036698	0.807935	-3136.176425	0.137257	-3136.301926	-3139.943986

XII. References

- (1) Li, J. L.; Sahoo, B.; Daniliuc, C. G.; Glorius, F. Conjugate umpolung of β,β -disubstituted enals by dual catalysis with an *N*-heterocyclic carbene and a Bronsted acid: facile construction of contiguous quaternary stereocenters. *Angew Chem., Int. Ed.* **2014**, *53*, 10515-9.
- (2) Mo, J.; Chen, X.; Chi, Y. R., Oxidative gamma-addition of enals to trifluoromethyl ketones: enantioselectivity control *via* Lewis acid/*N*-heterocyclic carbene cooperative catalysis. *J. Am. Chem. Soc.* **2012**, *134*, 8810-3.
- (3) Yang, H.; Sun, J.; Gu, W.; Tang, W. Enantioselective Cross-Coupling for Axially Chiral Tetra-ortho-Substituted Biaryls and Asymmetric Synthesis of Gossypol. *J. Am. Chem. Soc.* **2020**, *142*, 8036-8043.
- (4) Satpathi, B.; Ramasastry, S. S. Morita-Baylis-Hillman Reaction of β,β -Disubstituted Enones: An Enantioselective Organocatalytic Approach for the Synthesis of Cyclopenta[*b*]Annulated Arenes and Heteroarenes. *Angew. Chem., Int. Ed.* **2016**, *55*, 1777-1781.
- (5) Ghosh, A.; Patra, A.; Mukherjee, S.; Biju, A. T. Synthesis of 2-Aryl Naphthoquinones by the Cross-Dehydrogenative Coupling Involving an NHC-Catalyzed *endo*-Stetter Reaction. *J. Org. Chem.* **2019**, *84*, 1103-1110.
- (6) Mishra, U. K.; Patel, K.; Ramasastry, S. S. V. Synthesis of Cyclopropanoids *via* Substrate-Based Cyclization Pathways. *Org. Lett.* **2019**, *21*, 175-179.
- (7) Bannwarth, C.; Ehlert, S.; Grimme, S. GFN2-XTB - an Accurate and Broadly Parametrized Self-Consistent Tight-Binding Quantum Chemical Method with Multipole Electrostatics and Density-Dependent Dispersion Contributions. *J. Chem. Theory Comput.* **2019**, *15*, 1652-1671.
- (8) Grimme, S.; Bannwarth, C.; Shushkov, P. A Robust and Accurate Tight-Binding Quantum Chemical Method for Structures, Vibrational Frequencies, and Noncovalent Interactions of Large Molecular Systems Parametrized for All Spd-Block Elements ($Z = 1-86$). *J. Chem. Theory Comput.* **2017**, *13*, 1989-2009.
- (9) Bannwarth, C.; Caldeweyher, E.; Ehlert, S.; Hansen, A.; Pracht, P.; Seibert, J.; Spicher, S.; Grimme, S. Extended <sc>tight-binding</sc> Quantum Chemistry Methods. *WIREs Comput. Mol. Sci.* **2020**.
- (10) Zhao, Y.; Truhlar, D. G. The M06 Suite of Density Functionals for Main Group Thermochemistry, Thermochemical Kinetics, Noncovalent Interactions, Excited States, and Transition Elements: Two New Functionals and Systematic Testing of Four M06-Class Functionals and 12 Other Function. *Theor. Chem. Acc.* **2008**, *120*, 215-241.
- (11) Weigend, F.; Ahlrichs, R. Balanced Basis Sets of Split Valence, Triple Zeta Valence and Quadruple Zeta Valence Quality for H to Rn: Design and Assessment of Accuracy. *Phys. Chem. Chem. Phys.* **2005**, *7*, 3297-3305.
- (12) Weigend, F. Accurate Coulomb-Fitting Basis Sets for H to Rn. *Phys. Chem. Chem. Phys.* **2006**, *8*, 1057-1065.
- (13) Frisch, M. J.; Trucks, G. W.; Schlegel, H. B.; Scuseria, G. E.; Robb, M. A.; Cheeseman, J. R.;

- Scalmani, G.; Barone, V.; Mennucci, B.; Petersson, G. A.; Nakatsuji, H.; Caricato, M.; Li, X.; Hratchian, H. P.; Izmaylov, A. F.; Bloino, J.; Zheng, G.; Sonnenberg, J. L.; Hada, M.; Ehara, M.; Toyota, K.; Fukuda, R.; Hasegawa, J.; Ishida, M.; Nakajima, T.; Honda, Y.; Kitao, O.; Nakai, H.; Vreven, T.; Montgomery, J. A., Jr.; Peralta, J. E.; Ogliaro, F.; Bearpark, M.; Heyd, J. J.; Brothers, E.; Kudin, K. N.; Staroverov, V. N.; Keith, T.; Kobayashi, R.; Normand, J.; Raghavachari, K.; Rendell, A.; Burant, J. C.; Iyengar, S. S.; Tomasi, J.; Cossi, M.; Rega, N.; Millam, J. M.; Klene, M.; Knox, J. E.; Cross, J. B.; Bakken, V.; Adamo, C.; Jaramillo, J.; Gomperts, R.; Stratmann, R. E.; Yazyev, O.; Austin, A. J.; Cammi, R.; Pomelli, C.; Ochterski, J. W.; Martin, R. L.; Morokuma, K.; Krzewski, V. G.; Voth, G. A.; Salvador, P.; Dannenberg, J. J.; Dapprich, S.; Daniels, A. D.; Farkas, O.; Foresman, J. B.; Ortiz, J. V.; Cioslowski, J.; Fox, D. J. Gaussian 16, rev. A.03.; Gaussian, Inc.: Wallingford, CT, 2016.
- (14) Marenich, A. V.; Cramer, C. J.; Truhlar, D. G. Universal Solvation Model Based on Solute Electron Density and on a Continuum Model of the Solvent Defined by the Bulk Dielectric Constant and Atomic Surface Tensions. *J. Phys. Chem. B.* **2009**, *113*, 6378-6396.
- (15) Funes-Ardoiz, I.; Paton, R. S. GoodVibes v1.0.1 <http://doi.org/10.5281/zenodo.56091>.
- (16) Grimme, S. Supramolecular Binding Thermodynamics by Dispersion-Corrected Density Functional Theory. *Chem. Eur. J.* **2012**, *18*, 9955-9964.
- (17) Contreras-García, J.; Johnson, E. R.; Keinan, S.; Chaudret, R.; Piquemal, J. P.; Beratan, D. N.; Yang, W. NCIPLOT: A Program for Plotting Noncovalent Interaction Regions. *J. Chem. Theory Comput.* **2011**, *7*, 625-632.
- (18) Schrödinger, L. The PyMOL Molecular Graphics Development Component, Version 1.8; 2015.
- (19) Brethomé, A. V.; Fletcher, S. P.; Paton, R. S. Conformational Effects on Physical-Organic Descriptors: The Case of Sterimol Steric Parameters. *ACS Catal.* **2019**, *9*, 2313-2323.
- (20) Cezar, H. M. Clustering Traj <https://github.com/hmcezar/clustering-traj>.
- (21) Ho, J. Are Thermodynamic Cycles Necessary for Continuum Solvent Calculation of PK a s and Reduction Potentials? *Phys. Chem. Chem. Phys.* **2015**, *17*, 2859-2868.
- (22) Marenich, A. V.; Ho, J.; Coote, M. L.; Cramer, C. J.; Truhlar, D. G. Computational Electrochemistry: Prediction of Liquid-Phase Reduction Potentials. *Phys. Chem. Chem. Phys.* **2014**, *16*, 15068-15106.
- (23) Roth, H. G.; Romero, N. A.; Nicewicz, D. A. Experimental and Calculated Electrochemical Potentials of Common Organic Molecules for Applications to Single-Electron Redox Chemistry. *Synlett* **2016**, *27*, 714-723.
- (24) Zhang, X.; Paton, R. S. Stereoretention in Styrene Heterodimerisation Promoted by One-Electron Oxidants. *Chem. Sci.* **2020**, *11*, 9309-9324.
- (25) Isse, A. A.; Gennaro, A. Absolute Potential of the Standard Hydrogen Electrode and the Problem of Interconversion of Potentials in Different Solvents. *J. Phys. Chem. B.* **2010**, *114*, 7894-7899.
- (26) Zhang, M.; Wang, Y.; Li, S. J.; Wang, X.; Shi, Q.; Li, X.; Qu, L. B.; Wei, D.; Lan, Y. Multiple Functional Organocatalyst-Promoted Inert C-C Activation: Mechanism and Origin

- of Selectivities. *ACS Catal.* **2021**, *11*, 3443-3454.
- (27) Zhang, M.; Wang, X.; Yang, T.; Qiao, Y.; Wei, D. Theoretical Model for *N*-Heterocyclic Carbene-Catalyzed Decarboxylation Reactions. *Org. Chem. Front.* **2021**, *8*, 3268-3273.